



OPEN

Dynamics of a diffusive model for cancer stem cells with time delay in microRNA-differentiated cancer cell interactions and radiotherapy effects

Frank Eric Essongo¹, Alain Mvogo^{2✉} & Germain Hubert Ben-Bolie¹

Understand the dynamics of cancer stem cells (CSCs), prevent the non-recurrence of cancers and develop therapeutic strategies to destroy both cancer cells and CSCs remain a challenge topic. In this paper, we study both analytically and numerically the dynamics of CSCs under radiotherapy effects. The dynamical model takes into account the diffusion of cells, the de-differentiation (or plasticity) mechanism of differentiated cancer cells (DCs) and the time delay on the interaction between microRNAs molecules (microRNAs) with DCs. The stability of the model system is studied by using a Hopf bifurcation analysis. We mainly investigate on the critical time delay τ_c , that represents the time for DCs to transform into CSCs after the interaction of microRNAs with DCs. Using the system parameters, we calculate the value of τ_c for prostate, lung and breast cancers. To confirm the analytical predictions, the numerical simulations are performed and show the formation of spatiotemporal circular patterns. Such patterns have been found as promising diagnostic and therapeutic value in management of cancer and various diseases. The radiotherapy is applied in the particular case of prostate model. We calculate the optimum dose of radiation and determine the probability of avoiding local cancer recurrence after radiotherapy treatment. We find numerically a complete eradication of patterns when the radiotherapy is applied before a time $t < \tau_c$. This scenario induces microRNAs to act as suppressors as experimentally observed in prostate cancer. The results obtained in this paper will provide a better concept for the clinicians and oncologists to understand the complex dynamics of CSCs and to design more efficacious therapeutic strategies to prevent the non-recurrence of cancers.

Keywords Cancer cells, Cancer stem cells, MicroRNAs, Hopf bifurcation, Time delay, Circular patterns, Radiotherapy

Cancer cells result of abnormal growth and uncontrolled division of normal cells¹. Cancers grow from stem cells in the way that healthy organs do. The discovery of the existence of cancer stem cells (CSCs) in cancers has led to an understanding the mechanisms of cancer proliferation and development. The CSCs have been identified and isolated in many so-called solid tumors such as breast cancer, pancreatic cancer, glioblastoma (a type of brain cancer) and colon adenocarcinoma². Recent reports, primarily for haematopoietic malignancies, have suggested that CSCs can be selectively targeted without ablating normal stem cell function. The CSCs can be more resistant to chemotherapy and radiotherapy³. Sometimes, after cancer treatment, the cancer comes back or recurs, this is called a cancer recurrence. The CSCs are a minor population of tumor cells that possess the stem cell property of self-renewal. Dysregulation of stem cell self-renewal is likely requirement for the development of cancer⁴. The CSCs are biologically unique cells within a tumor, possessing self renewal capacity and produce progeny with self proliferative capacity, similar to normal stem cells⁵. All these properties have led many researchers to believe that CSCs are responsible for the recurrence and spread of glioblastoma and other cancers, since they give rise to multiple other cancer cells and produce new tumors⁶.

¹Laboratory of Nuclear Physics, Dosimetry and Radiation Protection, Department of Physics, Faculty of Science, University of Yaounde I, P.O. Box 812, Yaounde, Cameroon. ²Laboratory of Biophysics, Department of Physics, Faculty of Science, University of Yaounde I, P.O. Box 812 Yaounde, Cameroon. ✉email: mvogal_2009@yahoo.fr

MicroRNA molecules (MicroRNAs) are small non-coding RNA molecules that regulate gene expression by binding to RNA messenger, thereby preventing its translation into proteins⁷. The microRNAs are key regulators of the activity of CSCs and are also involved in the transformation of differentiated cancer cells (DCs) into CSCs^{8,9}. The DCs are tumor cells that undergo a process of differentiation, meaning they acquire specific characteristics to particular type of tissue. The microRNAs play an important role in many biological processes, including development, cell differentiation, and tumor progression. Similarly, complex cellular secretions (serum, plasma, urine, saliva, blood) are regulated by microRNAs in extracellular environment. The microRNAs are used as powerful biomarkers^{10–12}, of various human pathologies precisely when measured in the bloodstream. For example, the detection of abnormal levels of microRNAs in the blood of cancer patients makes them a very promising diagnostic tool in cancerology. In adrenocortical carcinomas or adrenocorticalomas, miRNAs are used as non-invasive molecular markers for prognostic evaluation within a very short time after surgery. It has been shown in¹³ that microRNA-483-5p is significantly more abundant in the serum of patients who have recurred within 3 years after surgery compared to those who have not recurred. Some researchers have found that a specific microRNA can act as an oncogene in some types of cancer while the same microRNA can also act as a cancer cell suppressor in other cancers. For example, the microRNA-29 molecule acts as a tumour suppressor in lung tumours and as an oncogene in breast cancer^{14,15}.

The CSCs are responsible to the tumor relapse, and their dynamics are closely linked to disease progression. Therefore, there is an urgent need for improved diagnostic methods that provide more precise clinical assessments and sensitive detection of symptoms at earlier stage of the disease. In this context, mathematical modeling has been successfully applied. For example, Bonnet and Dick¹⁶ have shown in a mathematical model that acute myeloid leukemia is indeed organized as a hierarchy, with the disease originating from a primitive hematopoietic cell. Wang et al.¹⁷ have studied network-based methods for the identification of microRNA-target pairs in cancer. A long the same line, Konstorum et al.¹⁸ demonstrated that feedback regulation in a model for CSCs can cause an allee effect. On this background, Olmeda and Amar¹⁹ investigated clonal pattern dynamics in the concept of CSCs and showed that disordered patterns can be obtained inside a stable growing contour driven by the cancer stem cells. Very recently, Mori and Amar²⁰ studied the importance of stochasticity and drug effects in a dynamical model for CSCs. These above-mentioned works implicitly assume that biological transitions such as the interactions between DCs or CSCs with signaling molecules and proteins are instantaneous. However, in reality these take time. Time delays play an important role in the modeling of life phenomena in various fields of applications^{21–23}. Time delays are often associated with complex molecular mechanisms, such as the activation of specific signaling pathways or the regulation of gene expression by microRNAs.

In this paper, we investigate a diffusive model for tumor initiation composed of CSCs, DCs and other cells that do not contribute significantly to the dynamics of the tumor, such as dead, quiescent and healthy cells. The dynamical system is based on the proliferation rates controlled by chemical pathways and physical interaction for each cell population. It mainly takes into account the diffusion of cells, the de-differentiation (or plasticity) mechanism of differentiated cancer cells (DCs) and the time delay on molecule-cell interaction of microRNAs with DCs. We propose an efficiency mathematical approach that includes the radiotherapy effects. Radiotherapy is one of the most commonly used treatments for cancer, and its effectiveness largely depends on the sensitivity of cancer cells to radiation²⁴. We show that the radiotherapy can be applied before a certain critical time delay in the dynamical system for a complete eradication of the tumor. This critical time delay represents the time from which some DCs transform into CSCs. The rest of the paper is organized as follows. In “[The diffusive model with time delay and linear stability analysis](#)” section, we present the model formulation and perform the linear stability analysis. We calculate the value of critical time delay for 3 different cancer models, namely prostate, lung and breast cancers. In “[Analytical and numerical results](#)” section, we integrate the radiotherapy function in the model and some analytical and numerical results are presented and discussed. “[Discussion and conclusion](#)” section concludes the paper.

The diffusive model with time delay and linear stability analysis

Model formulation

There are a number of mathematical models used to describe the dynamics of cancer stem cells (CSCs). These models include the Dick's model¹⁶, the Reya's model²⁵ and many others^{26–28}. The model investigated in this paper is the one proposed by Konstorum et al.¹⁸ and improved by Olmeda and Amar¹⁹ and Mori and Amar²⁰. The mathematical model considers the dynamics of three types of cells: CSCs with similar characteristics as normal stem cells or progenitor cells such as self-renewal ability and multi-lineage differentiation to drive tumor growth and heterogeneity, differentiated cancer cells (DCs) which are specific to the tumor and vary across organs and other cells (C) or inert constituents. The CSCs are the sub-populations that undergo cell division leading for the proliferation of cells. The model also considers eliminating intermediate progenitors to the proliferation process. A CSC can divide symmetrically into two CSCs or two DCs, or asymmetrically into one CSC and one DC. The average number of CSCs generated in division is regulated by an activator Wnt- β (Wingless-related integration site) catenin pathway proteins⁸ with concentration a . Experimental evidence shows that a feedback mechanism exists, triggered by phenotypic changes of DCs that revert to the CSC state. This process, also known as cancer cell plasticity, is driven by an activator microRNA molecules (microRNAs) with concentration m ⁹. It is now proved that differential dynamical systems with time delay and diffusion play an important role in the modeling of real life phenomena in biology, physics and medicine^{21–23,29–31}. Also, the modeling of CSCs with diffusion has the potential to yield invaluable insights into cancer metastasis, disease progression, and treatment efficacy assessment³². Then, to improve the model, we include the diffusion process in the dynamical equations of all types of cells and molecules. More interesting, we include a time delay τ in the dynamical equation of CSCs to

represent the time needed for DCs to produce new CSCs after the interaction of microRNAs with DCs. All these assumptions can be explained in the following set of equations:

$$\begin{cases} \frac{dS}{dt} = (2p(D, a) - 1)\varepsilon S + q(m(t - \tau))D(t - \tau) + D_S \Delta S, \\ \frac{dD}{dt} = 2(1 - p(D, a))\varepsilon S - (d + q(m))D + D_D \Delta D, \\ \frac{da}{dt} = a\beta S \frac{a}{1+a} - \alpha + D_a \Delta a, \\ \frac{dm}{dt} = \gamma e^{-S/S_0} - \alpha m + D_m \Delta m, \end{cases} \quad (1)$$

where $S = S(x, y, t)$ is the concentration of CSCs, $D = D(x, y, t)$ is the concentration of DCs, $a = a(x, y, t)$ represents the concentration of Wnt- β catenin pathway proteins and $m = m(x, y, t)$ the concentration of microRNAs. The quantities $2p(D, a)$ denotes the probability to gain two CSCs per mitosis and $q(m(t - \tau))$ represents the DCs dedifferentiation rate. They satisfy:

$$p(D, a) = \frac{\eta a}{(1 + \eta a)(1 + \psi D)}, \quad q(m(t - \tau)) = \frac{q_0}{2} \left(1 + \tanh \left(\frac{m(t - \tau) - m_0}{\sigma} \right) \right), \quad (2)$$

where the parameter q_0 represents the maximum conversion rate per year of DCs into CSCs and m_0 the tiny concentration of microRNAs. The parameters α, β respectively represent the degradation rate of proteins, controlling the aggressiveness of self-renewal Wnt- β catenin pathway proteins. The parameter σ measures the sensitivity of CSCs when interacting with microRNAs. The parameter η refers to the definition of a probability coefficient $p(D, a)$ for the inhibitor produced by D cells, where ψ gives the intensity of the brake. The parameter d is the differentiated cancer cells death rate ($d > 0$). The parameter ε represents a time unit the inverse of the mitotic rate of the CSCs. The quantity S_0 is a tiny fraction of S of the entire tumor population. In practice when S is below S_0 , the activator m starts to grow as $q(m)$, leading to an increase of S . Indeed, when m stimulates DCs that possess plasticity, the DCs transform into CSCs over a period of time. Given this process, we have considered a time delay τ which represents the time needed for DCs to produce CSCs after the interaction with microRNAs. In practice, time delays in biological systems may be large³³. The term Δ is the Laplacian operator in two dimensions, such that $\Delta = \frac{\partial^2}{\partial x^2} + \frac{\partial^2}{\partial y^2}$.

From biological considerations, we assume: $S \geq 0, D \geq 0, a \geq 0, m \geq 0, (x, y) \in \Sigma = (0, L) \times (0, L)$ and we use zero-flux boundary conditions: $\frac{\partial S}{\partial \varpi} |_{\partial \Sigma} = \frac{\partial D}{\partial \varpi} |_{\partial \Sigma} = \frac{\partial a}{\partial \varpi} |_{\partial \Sigma} = \frac{\partial m}{\partial \varpi} |_{\partial \Sigma} = 0$. The main reason for choosing such boundary conditions is that we are interested in the self-organization of pattern and zero-flux conditions imply no external input. The length of $x, y \in (0, L)$ is measured in millimeter [mm], where the length scale L denotes the size of the system in square domain and ϖ is the outward unit normal vector of the boundary $\partial \Sigma$. In practice, the length scale L is the average penetration depth of cells in tissue. The time is measured in years. The units of variables and parameters used in this paper are given in the Table 1.

Linear stability analysis

The linear stability analysis is attributed to the highest sensibility of biological system³⁷. The linear stability analysis deals with infinitesimal perturbation and consists to perturb the steady state of the system. It is easy to check that system (1) has three equilibrium points, $E^{(1)} = (0, 0, 0, m_1), E^{(2)} = (S_2, D_2, 0, m_2)$ and $E^{(3)} = (S_3, D_3, a_3, m_3)$.

The first steady state of system (1) is $E^{(1)} = (0, 0, 0, m_1)$, that is, $S = 0, D = 0, a = 0$ and m_1 an arbitrary value. Notice that the equilibrium $E^{(1)}$ corresponds to the hypothetical situation where there is no CSCs, no DCs and the Wnt- β protein is inactive.

The second steady state is $E^{(2)} = (S_2, D_2, 0, m_2)$, that is, $S_2 = -S_0 \text{Log} \left(\frac{\alpha m_2}{\gamma} \right), D_2 = \frac{S_2}{d}, a_2 = 0$ and m_2 an arbitrary value. $E^{(2)}$ is biologically meaningful and $E^{(2)}$ corresponds to the situation where Wnt- β protein is inactive and the microRNAs has arbitrary values. This equilibrium point is always stable if $d < q_0$ and $m_2 < \frac{\gamma}{\alpha}$.

The third steady state $E^{(3)} = (S_3, D_3, a_3, m_3)$, that is, $S_3 = \frac{\alpha(1+a_3)}{\beta a_3}, D_3 = \frac{\alpha(1+a_3)}{\beta d a_3}, m_3 = \frac{\gamma}{\alpha} e^{-S_3/S_0}$ and $a_3 = \frac{1 + \frac{\psi \alpha}{d \beta} (1 + \eta)}{2\eta(1 - \frac{\psi \alpha}{d \beta})} \left(1 + \sqrt{1 + \frac{4 \frac{\psi \alpha}{d \beta} \eta (1 - \frac{\psi \alpha}{d \beta})}{(1 + \frac{\psi \alpha}{d \beta} (1 + \eta))^2}} \right)$. E^3 is an unstable equilibrium point. Biologically, E^3 corresponds to

the case where the wnt- β catenin signaling pathway and microRNAs are activated, leading to uncontrolled proliferation of cancer stem cells. This also can be related to the chronic phase of the disease. Our goal is to study the phenomenon of conversion of differentiated cancer cells into cancer stem cells influenced by microRNAs when the wnt- β signaling pathway is not activated. At this stage, cancer proliferation can be controlled and the patient can be treated if appropriate therapeutic strategies are used. In the rest of the paper, for the biomedical view point, we will investigate the dynamics of the system at the stable equilibrium point $E^{(2)}$.

We now explore the dynamics of diffusion-driven instability with respect to $E^{(2)}$. For this, consider small spatiotemporal perturbations $\delta S(x, y, t), \delta D(x, y, t), \delta a(x, y, t)$ and $\delta m(x, y, t)$ on homogenous steady state $E^{(2)} = (S_2, D_2, 0, m_2)$ so that we have:

$$\begin{aligned} S(x, y, t) &= S_2 + \delta S(x, y, t); & D(x, y, t) &= D_2 + \delta D(x, y, t), \\ a(x, y, t) &= 0 + \delta a(x, y, t); & m(x, y, t) &= m_2 + \delta m(x, y, t). \end{aligned} \quad (3)$$

Expressing spatiotemporal perturbations in the form:

Variable	Description	Unit adopted	
<i>S</i>	Concentration of CSCs	cell.mm ⁻³	
<i>D</i>	Concentration of DCs	cell.mm ⁻³	
<i>a</i>	Concentration of Wnt-β	molecule.mm ⁻³	
<i>m</i>	Concentration of microRNAs	molecule.mm ⁻³	
Parameter	Description	Value & Unit	References
<i>η</i>	Positive feedback strength of Wnt-β	1 mm ³ .molecule ⁻¹	Modified from ¹⁹
<i>ψ</i>	Negative feedback strength of DCs	0.5 mm ³ .cell ⁻¹	Modified from ³⁴
<i>ε</i>	Mitotic rate of the CSCs	1 year ⁻¹	Modified from ²⁰
<i>q</i>	DCs dedifferentiation rate	year ⁻¹	¹⁹
<i>q</i> ₀	Maximum DCs dedifferentiation rate	<i>q</i> ₀ > <i>d</i> year ⁻¹	¹⁹
<i>m</i> ₀	Minimal concentration of microRNAs	0.05 molecule.mm ⁻³	Modified from ¹⁹
<i>d</i>	DCs death rate	36.5–109.5 year ⁻¹	²⁰
<i>α</i>	Degradation rate of proteins or molecules	0.3 mm ³ .molecule ⁻¹	Modified from ³⁵
<i>β</i>	Aggressiveness of self-renewal Wnt-β rate	1 mm ³ .cell ⁻¹ .year ⁻¹	Modified from ³⁵
<i>γ</i>	Maximum concentration of microRNAs	1 molecule.mm ⁻³ .year ⁻¹	Modified from ¹⁹
<i>σ</i>	Sensitivity of CSCs when interacting with microRNAs	0.05 molecule.mm ⁻³	Modified from ¹⁹
<i>S</i> ₀	Minimal concentration of CSCs	0.038 cell.mm ⁻³	Modified from ¹⁹
<i>D</i> _S	Diffusion coefficient of CSCs	0.031536 mm ² .year ⁻¹	³⁶
<i>D</i> _D	Diffusion coefficient of DCs	0.031536 mm ² .year ⁻¹	³⁶
<i>D</i> _a	Diffusion coefficient of Wnt-β	0.365 mm ² .year ⁻¹	¹³
<i>D</i> _m	Diffusion coefficient of microRNAs	0.365 mm ² .year ⁻¹	¹³

Table 1. Variables and parameters of the model.

$$\begin{aligned} \delta S(x, y, t) &= \delta S_2 e^{\lambda t} \cos k_x x \cos k_y y; & \delta D(x, y, t) &= \delta D_2 e^{\lambda t} \cos k_x x \cos k_y y, \\ \delta a(x, y, t) &= \delta a_2 e^{\lambda t} \cos k_x x \cos k_y y; & \delta m(x, y, t) &= \delta m_2 e^{\lambda t} \cos k_x x \cos k_y y, \end{aligned} \tag{4}$$

where λ is the growth rate of the perturbation in time t . The parameters δS_2 , δD_2 , δa_2 and δm_2 represent the amplitudes, and k_x and k_y are the wavenumbers in the x and y directions, respectively. Inserting Eqs. (3) and (4), we obtain the following matrix equation for eigenvalues

$$\begin{pmatrix} -1 - D_S k^2 - \lambda & d e^{-\lambda \tau} & \frac{2S_2 \eta}{1 + \psi D_2} & \frac{2dD_2}{\sigma} \left(1 - \frac{d}{q_0}\right) e^{-\lambda \tau} \\ 2 & -2d - D_D k^2 - \lambda & -\frac{2S_2 \eta}{1 + \psi D_2} & -\frac{2dD_2}{\sigma} \left(1 - \frac{d}{q_0}\right) \\ 0 & 0 & -\alpha - D_a k^2 - \lambda & 0 \\ -\frac{\alpha}{S_0} m_2 & 0 & 0 & -\alpha - D_m k^2 - \lambda \end{pmatrix} = 0.$$

The eigenvalues λ are the solutions of the quadratic equation as follows:

$$\lambda_k^4 + C_{11} \lambda_k^3 + C_{22} \lambda_k^2 + C_{33} \lambda_k + C_{44} + (E_{11} \lambda_k^2 + E_{22} \lambda_k + E_{33}) e^{-\lambda_k \tau} = 0, \tag{5}$$

where the parameters C_{11} , C_{22} , C_{33} , C_{44} , E_{11} , E_{22} and E_{33} are given in Online Appendix.

Let $i\omega_k$ (where ω_k is positive) be the root of Eq. (5) and separating the real and imaginary parts, we obtain the following system of equations:

$$\begin{cases} C_{22} \omega_k^2 - C_{44} - \omega_k^4 = E_{22} \omega_k \sin \omega_k \tau + (E_{33} - E_{11} \omega_k^2) \cos \omega_k \tau, \\ C_{33} \omega_k - C_{11} \omega_k^3 = (E_{33} - E_{11} \omega_k^2) \sin \omega_k \tau - E_{22} \omega_k \cos \omega_k \tau. \end{cases} \tag{6}$$

From Eq. (6), we obtain

$$\begin{cases} \cos \omega_k \tau = \frac{(E_{33} - E_{11} \omega_k^2)(C_{22} \omega_k^2 - C_{44} - \omega_k^4) - E_{22} \omega_k (C_{33} \omega_k - C_{11} \omega_k^3)}{(E_{33} - E_{11} \omega_k^2)^2 + E_{22}^2 \omega_k^2}, \\ \sin \omega_k \tau = \frac{E_{22} \omega_k (C_{22} \omega_k^2 - C_{44} - \omega_k^4) + (E_{33} - E_{11} \omega_k^2)(C_{11} \omega_k^3 - C_{33} \omega_k)}{(E_{33} - E_{11} \omega_k^2)^2 + E_{22}^2 \omega_k^2}, \end{cases} \tag{7}$$

which leads to

$$\omega_k^8 + (C_{11}^2 - 2C_{22})\omega_k^6 + (C_{22}^2 + 2C_{44} - 2C_{11}C_{33} - E_{11}^2)\omega_k^4 + (C_{33}^2 + 2E_{11}E_{33} - 2C_{22}C_{44} - E_{22}^2)\omega_k^2 + (C_{44}^2 - E_{33}^2) = 0. \tag{8}$$

We now suppose that (8) has at least one positive root. Then, (8) has a positive root $\omega_k = \omega^*$ such that (5) has a pair of purely imaginary roots $\pm i\omega_k$. Then, we can obtain the corresponding critical value of the delay for ω_k

$$\tau_k^{(j)} = \begin{cases} \frac{1}{\omega_k} \arctan\left(\frac{Z_{11}^k}{Z_{22}^k}\right) + \frac{j2\pi}{\omega_k}, & \text{if } Z_{11}^k > 0 \\ \frac{1}{\omega_k} \left[\pi + \arctan\left(\frac{Z_{11}^k}{Z_{22}^k}\right) \right] + \frac{j2\pi}{\omega_k}, & \text{if } Z_{22}^k < 0 \\ \frac{1}{\omega_k} \left[2\pi + \arctan\left(\frac{Z_{11}^k}{Z_{22}^k}\right) \right] + \frac{j2\pi}{\omega_k}, & \text{if } Z_{11}^k < 0, Z_{22}^k > 0, \end{cases} \tag{9}$$

where $j = 0, 1, 2, \dots$ from (12), $Z_{11}^k = E_{22}\omega_k(C_{22}\omega_k^2 - C_{44} - \omega_k^4) + (E_{33} - E_{11}\omega_k^2)(C_{11}\omega_k^3 - C_{33}\omega_k)$ and $Z_{22}^k = (E_{33} - E_{11}\omega_k^2)(C_{22}\omega_k^2 - C_{44} - \omega_k^4) - E_{22}\omega_k(C_{33}\omega_k - C_{11}\omega_k^3)$.

Differentiating both sides of Eq. (8) with respect to τ , we obtain

$$\left[\frac{d\lambda_k}{d\tau} \right]^{-1} = \frac{4\lambda_k^3 + 3C_{11}\lambda_k^2 + 2C_{22}\lambda_k + C_{33} + (2E_{11}\lambda_k + E_{22})e^{-\lambda_k\tau}}{\lambda_k(E_{11}\lambda_k^2 + E_{22}\lambda_k + E_{33})e^{-\lambda_k\tau}} - \frac{\tau}{\lambda_k},$$

which yields, at $\tau = \tau_c = \tau_k^{(j)}$, the following transversality condition :

$$\text{signRe} \left[\frac{d\lambda_k}{d\tau} \right]_{\tau=\tau_c} = \text{Re} \left[\frac{d\lambda_k}{d\tau} \right]_{\tau=\tau_c}^{-1} = \text{sign} \left(\frac{\tilde{A}_R \tilde{B}_R + \tilde{A}_I \tilde{B}_I}{\tilde{B}_R^2 + \tilde{B}_I^2} \right) > 0, \tag{10}$$

where

$$\begin{cases} \tilde{B}_R = -E_{22}\omega^2 \cos \omega\tau_c + (-E_{11}\omega^3 + E_{33}\omega) \sin \omega\tau_c, \\ \tilde{B}_I = (E_{33}\omega - E_{11}\omega^3) \cos \omega\tau_c + E_{22}\omega^2 \sin \omega\tau_c, \\ \tilde{A}_R = E_{22} \cos \omega\tau_c - 3C_{11}\omega^2 + 2E_{11}\omega \sin \omega\tau_c + C_{33}, \\ \tilde{A}_I = -4\omega^3 + 2E_{11}\omega \cos \omega\tau_c + 2C_{22}\omega - E_{22}\sin \omega\tau_c. \end{cases} \tag{11}$$

The transversality condition is a mathematical requirement to ensure the validity of the model. In the case of the model under study, the transversality condition must be greater than zero. This means that the critical time delay, which represents the time delay after which a differentiated cancer cell converts to a cancer stem cell, must be strictly positive. We recall that when $\tau = 0$ equilibrium $E^{(2)}$ is always stable when $(d < q_0)$ and $(m_2 < \frac{\gamma}{\alpha})$.

From, the transversality condition (10) for $\tau > \tau_c$, $E^{(2)}$ is unstable and stable for $\tau < \tau_c$.

When $\tau = \tau_c$, Hopf bifurcation occurs.

Analytical and numerical results

Analytical results

In this section, we present some analytical results related with this work. We calculate the value of the critical time delay τ_c given in Eq. (9) for some cancers, namely prostate, lung and breast cancers. The estimated values of q_0 and d that we use are related to a cancer and taken in the literature. The results are summarized in Table 2.

We recall that the critical time delay τ_c represents the time for DCs to transform into CSCs after the interaction of microRNAs with DCs. At this time, the system becomes unstable. From the biological view point, this situation corresponds to the proliferation of CSCs indicating progression leading sometime to metastases¹⁴. The critical time delay values obtained in Table 2 can be also considered to the relapse period of cancer. For the breast cancer, $\tau_c = 0.5858$ year, and this value can correspond with the relapse period of triple-negative breast cancer⁴⁵. This type of breast cancer is characterized by the absence of over-expression of hormone receptors for estrogen and progesterone and absence of over-expression of the HER2 growth factor⁴⁵. Among the different types of breast cancer, triple-negative cancers are the ones that recur most frequently and more rapidly than other tumor types. In fact, between 6 and 24 months after the primary tumor, 52.3 percents of triple-negative metastases are discovered, 24 percents of metastases are discovered for HER2+ and 12 percent of metastases are discovered for HR+HER2-⁴⁶. For a lung cancer $\tau_c = 0.6287$ is less than 2 years and this time corresponds to an early recurrence observed in small cell lung cancer^{47,48}. For a prostate cancer $\tau_c = 11.8964$. This result confirm

Type of cancer	Values q_0 and d	Value of the critical time delay τ_c
Prostate cancer	$q_0 = 87.6 \text{ year}^{-1}, d = 87.2 \text{ year}^{-19,20,38}$	11.8964 years
Lung cancer	$q_0 = 109.97 \text{ year}^{-1}, d = 80 \text{ year}^{-139-41}$	0.6287 year
Breast cancer	$q_0 = 70.39 \text{ year}^{-1}, d = 45 \text{ year}^{-142,43}$	0.5858 year

Table 2. Value of the critical time delay τ_c for some cancers.

the one obtained by Pound et al.⁴⁹ who have shown that a very low recurrence of prostate cancer 11 years later is possible, and that 10 percents of men with undetectable prostate-specific antigen (PSA) levels 10 years after radical prostatectomy subsequently develop biochemical recurrence, which means an increase in the PSA levels without clinical signs of cancer. Therefore, an estimation of the recurrence period of cancer can be important to adjust therapeutic treatment and to take preventive measures to reduce the risk of recurrence.

Numerical results

We perform extensive numerical simulations of the spatially extended model (1) in two-dimension spaces in the case of prostate cancer model parameters. The numerical simulations employ a system size of 100×100 space units. The numerical integration of model (1) was performed in MATLAB by means of forward Runge-Kutta of fourth order with Hermite interpolation. This method is favored for its accuracy and stability compared to other numerical methods^{50,51}. A time step $\Delta t = 0.01$ and a space step of $\Delta x = \Delta y = 0.2$ are used. Further, the model (1) is investigated numerically under the zero flux boundary conditions. The choice of initial value indicates small inhomogeneous spatial perturbation from homogeneous equilibrium state $E^{(2)}$. The initial distribution of the populations are taken as

$$\begin{aligned} S(x, y, 0) &= S_2 + (-0.1\cos((x^2 + y^2)\pi - 0.01\sin((x^2 + y^2)\pi))), \\ D(x, y, 0) &= D_2 + (-0.0002\cos((\sqrt{x^2 + y^2})\pi + 0.0003\sin((\sqrt{x^2 + y^2})\pi))), \\ a(x, y, 0) &= a_2 + (0.002\cos(x + 2)^2 + 0.001\sin(y + 4)^2), \\ m(x, y, 0) &= m_2 + (0.001\cos(x - 2)^2 + 0.001\sin(y - 4)^2), \end{aligned}$$

where $\{(S_2, D_2, a_2, m_2)\} = \{(0.140000, 0.001605, 0.000000, 0.080000)\}$

To avoid numerical stiffness, we performed the simulations qualitatively for smaller values of the step sizes.

Bifurcation diagrams and time series

We now explore the bifurcation of the system, in order to show that the system can manifest diverse biological phenomena such as shifts in cell concentrations and cell-protein interactions. Figure 1 shows the emergence of bifurcation in the system. In this figure, the equilibrium state is represented by a stationary point where the system trajectory remains constant. Instability is indicated by the Hopf bifurcation and its occurs at the critical time delay $\tau_c = 11.8964$. In fact, when $\tau < \tau_c$, the system is stable at the equilibrium $E^{(2)}$ and when $\tau > \tau_c$, the system becomes unstable. From the biological point of view, the instability occurs at $\tau = \tau_c$, that is when the conversion of DCs into CSCs takes place indicating tumor progression. It is observed an increase in the concentration D of DCs and a decrease in the concentration m of microRNAs. Thus, the critical time delay τ_c can be viewed as the initial time for the proliferation of CSCs. Then, Hopf bifurcation indicates the transition to the disease state, characterized by the proliferation of CSCs²⁵. This bifurcation can serve as a crucial indicator of substantial disruptions in the system's normal functioning, with potentially implications for health and disease.

Figure 2 shows the time series of $S(t)$, $D(t)$ and $m(t)$. We observe that before the critical time delay $\tau_c = 11.8964$, the concentrations S and D of CSCs and of DCs, respectively decrease while the concentration m of microRNAs decreases as time progresses. For such a situation, it has been shown that the microRNAs can reduce tumorigenicity⁷. Some works reported also in vivo that the regulation of *NF90* greatly reduces ovarian tumor proliferation and invasion⁵². This regulation also greatly reduces the size of the ovarian tumor and the number of metastases. We also observe a dormancy period of cancer cells. From the biomedical view point, during this period the patients often have no symptoms and the tumor can be undetectable using the usual diagnostic tools such as PET scan (nuclear medicine imaging examination). After the time $\tau_c = 11.8964$, we observe the inverse

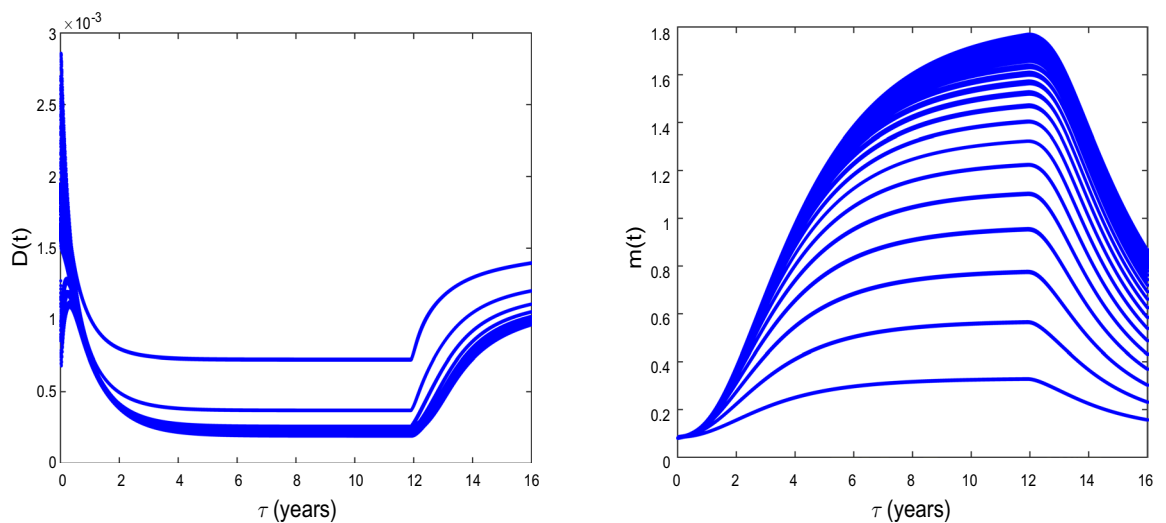


Figure 1. Bifurcation diagrams of $D(t)$ and $m(t)$. $D_S = D_D = 0.031536$ and $D_a = D_m = 0.365$ and the values of the other parameters values are given in the Table 1. We observe that Hopf bifurcation occurs at $\tau = \tau_c = 11.8964$ for prostate cancer.

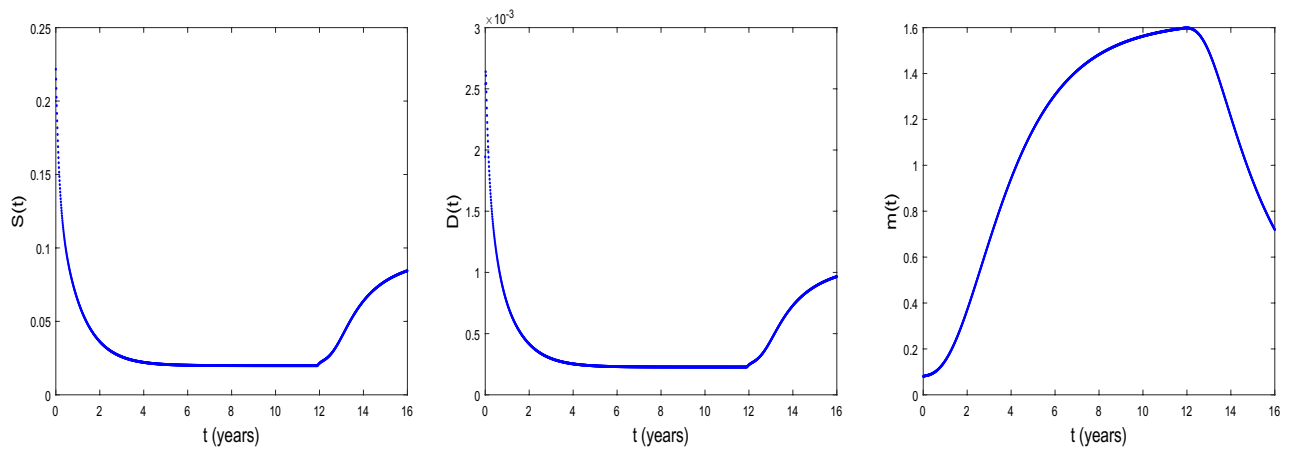


Figure 2. The time series of $S(t)$, $D(t)$, and $m(t)$ at $\tau = \tau_c = 11.8964$ for $D_S = D_D = 0.031536$ and $D_a = D_m = 0.365$. The other parameter values are given in the Table 1.

of the scenario, the concentration m decreases as time progresses while the concentrations S and D increase. In this case, oncogenic role for microRNAs can be reported.

Pattern formation and effect of diffusion on cancer cells

The diffusion of cancer stem cells is a complex phenomenon characterized by the migration and invasion of these cells from the primary tumor to distant organs, leading to the formation of metastases⁴⁴. This process, known as metastasis, is a major contributor to cancer-related deaths, as it confers resistance to treatment strategies and increases the risk of relapse⁵³. Therefore the effect of diffusion on cancer stem cells is an important to understand cancer mechanisms and develop new therapeutic strategies. The effect of diffusion on cancer stem cells could lead also to the development of a prevention strategy for non-recurrence in either non-metastatic or metastatic cancer.

Figure 3 shows the process of pattern formation for different values of diffusion coefficients at $\tau = \tau_c = 11.8964$.

The Fig. 3 exhibits the formation of circular patterns. Such circular patterns have great pre-clinical diagnostic and therapeutic potentials in multiple cancers. These have been reported playing important roles in multiple malignant behaviors including proliferation, migration, metastasis and chemoresistance⁵⁴. Pattern formation has been also observed in other biological systems to explain energy transport in DNA strands^{55,56}, impulse propagation in neural networks^{56,57} and instabilities in directed networks⁵⁸.

In Fig. 3a the patterns are obtained for $D_S = D_D = 0.0031536$ and $D_a = D_m = 0.0365$. The patterns in the spatial domain represent the distribution and density of cancer cells in different regions. Since the patterns are more localized in the center, it may indicate that the cancer cells can not migrate far from their origin. This can be related to non-metastasized behavior⁴⁴. In Fig. 3b, the patterns are obtained for the diffusion coefficients such that $D_S = D_D = 0.031536$ and $D_a = D_m = 0.365$ (we have increased the diffusion coefficients). We observe that the patterns are less localized in the center of the spatial domain. This may suggest that the cancer cells have

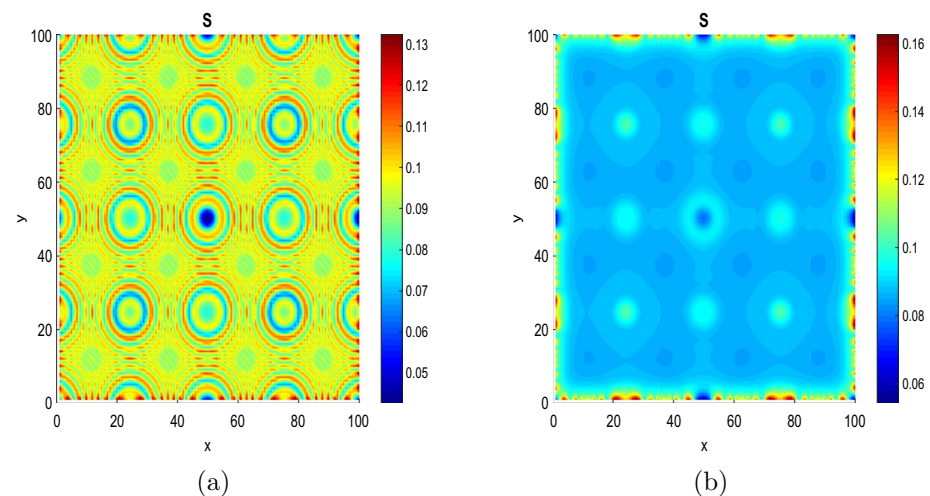


Figure 3. Panels show the feature of patterns at fixed parameters $\tau = \tau_c = 11.8964$ and time $t = 16$. (a) $D_S = D_D = 0.0031536$ and $D_a = D_m = 0.0365$ and (b) $D_S = D_D = 0.031536$ and $D_a = D_m = 0.365$.

dispersed widely and reached distant areas. Since metastasized behavior refers to the spread of cancer cells from their original site to other parts of the body. The scenario observed in this figure can be related to metastasized behavior. In this case, the function and structure of the surrounding tissues and organs can be affected⁴⁴.

Figure 4 shows the emergence of circular patterns in the system for the different species of the model. We assume the time delay $\tau = 6.8964$, which means 5 years before the dedifferentiation of DCs. Such circular patterns of CSCs, DCs and microRNAs obtained in this work have been observed in some solid tumors, where the CSCs surrounded by the DCs forming protective niche⁵⁹. Circular patterns of CSCs, DCs and microRNAs obtained can be used as biomarkers for diagnosis, by allowing to identify the type, stage and molecular subtype of the tumor. For example, circular pattern of microRNAs can be detected in blood, urine or biopsies of patients and can reflect the genetic profile of the tumor. Circular patterns of CSCs and DCs can be observed by imaging techniques such as positron emission tomography and can indicate the degree of aggressiveness and vascularization of the tumor⁵⁹. In addition to diagnosis, circular patterns of CSCs, DCs and microRNAs, can also be used as biomarkers for cancer prognosis, by allowing to evaluate the risk of recurrence, progression or metastasis of tumor. For example, circular pattern of microRNAs can be associated with the overall survival or disease-free survival of patients and can predict the response to treatments⁵⁴. Circular patterns of CSCs and DCs can be related to the invasive and metastatic potential of the tumor and can influence choice of treatment.

In Fig. 5, we assume the time $\tau = 14.8964$, which means 3 years after the dedifferentiation of DCs. As one can observe, after the dedifferentiation, these circular patterns become more localized. The emergence of localized circular patterns can also be the result of physical, chemical or biological processes. For example, at the molecular level, circular patterns can be observed in the structure of some molecules such as circular RNAs. At the cellular level, circular patterns can be involved in the dynamics of membranes. For example the formation of curvature, fission and sorting of lipids in the membranes can be influenced by proteins that induce circular patterns. At the tissue level, circular patterns can be associated with morphogenesis and differentiation. At the organ level, circular patterns can be related to circulation and respiration⁶⁰. Circular pattern are also important because of their prominence in virus DNA.

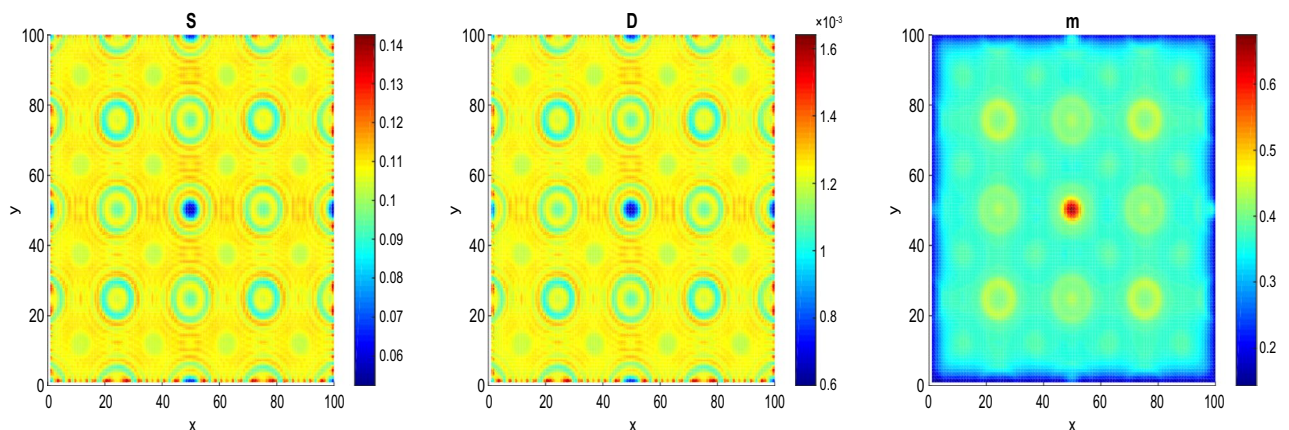


Figure 4. The process of formation of circular patterns for a value of $\tau = 6.8964 < \tau_c = 11.8964$ and the parameters $D_S = D_D = 0.0031536$, $D_a = D_m = 0.0365$, at time $t = 16$. The values of the other parameters are given in the Table 1.

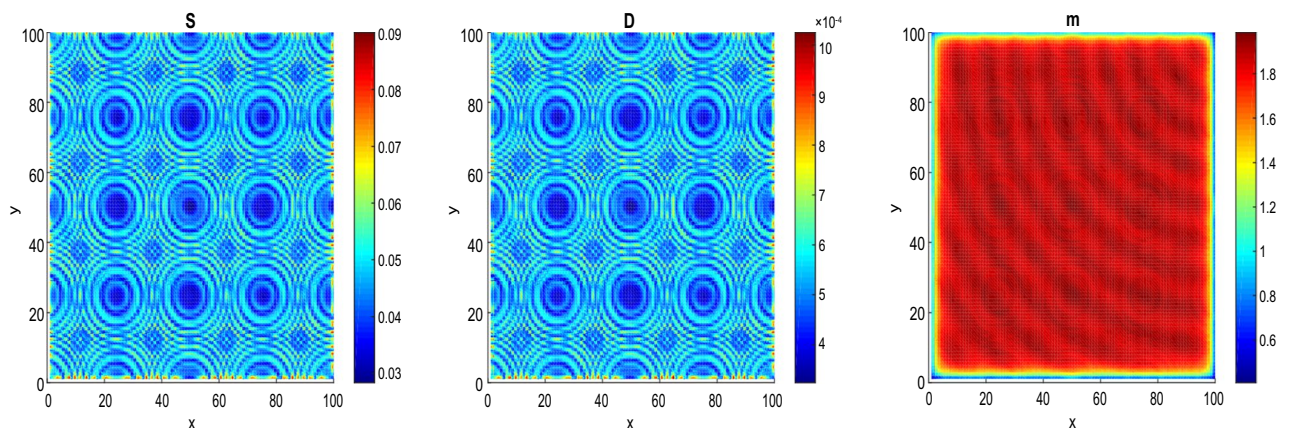


Figure 5. The process of formation of patterns at $\tau = 14.8964 > \tau_c = 11.8964$, $t = 16$, $D_S = D_D = 0.0031536$ and $D_a = D_m = 0.0365$. The values of the other parameters are given in the Table 1.

In addition to the fact that for the numerical point of view, colors in patterns generally represent different level of cell concentrations, from the biological point of view, the colors in circular patterns obtained in this work indicate that as genes recombine inside the cell, the cell elaborates a color unique to its genetic code. For cancer stem cells, that color becomes a genetic signature passed down to daughter cells. Blue stem cells, for example, will only make blue cancer cells. Along the same line, researchers at Harvard Medical School and Boston Children's Hospital reported a new color-coding tool enabling scientists to better track live blood stem cells over time, a key part of understanding how blood disorders and such cancers as leukemia arise⁶¹.

Radiotherapy modeling and effects

In this section, we focus on the radiotherapy effects on the dynamical system (1). Radiation induced cell death. Radiation directly affects DNA molecule in the target tissue, single broken strand can usually be repaired by the cell while two broken strands commonly result in cell death. We know that it is possible to identify, isolate and quantify CSCs in a large number of cancers including brain, colon, prostate, lung, breast, blood⁶². Several studies^{63–65} have shown that CSCs are resistant to cytotoxic treatments such as radiotherapy. For example, numerous studies have demonstrated the high resistance of CSCs to in vitro exposure to single-dose, low LET ionizing radiation and chemotherapy. However, the effects of fractionated radiation on CSCs have not been sufficiently studied. We will examine through numerical simulations the behavior of the system when irradiated with X-rays before resurgence using fractionated doses. Radiation fractionated therapy for treatment of cancer has many advantages over single radiation administration as it raises the effect of anticancer therapy and decreases the chances of side effects occurrence in normal tissues. The dose fractionation in radiotherapy is a technique that involves dividing the total radiation dose into several smaller sessions, called fractions. This approach is used to treat cancer patients with a higher radiation dose while minimizing side effects on the surrounding normal tissues. The importance of dose fractionation in radiotherapy lies in several key aspects namely protection of normal tissues, by dividing the total dose into smaller fractions. It allows healthy tissues to recover between sessions, thus reducing undesirable side effects. This can improve treatment efficacy by causing more damage to cancer cells. Dose fractionation allows physicians to personalize treatment based on specific patient characteristics, such as tumor size and location, as well as individual tolerance to side effects. It is important to note that dose fractionation may vary depending on the type and stage of cancer, tumor location and treatment goals. We now consider $R = R(t)$ the radiotherapy function. Introducing R in the first equation of system (1), we obtain the following system:

$$\begin{cases} \frac{dS}{dt} = (2p(D, a) - 1)S + q(m(t - \tau))D(t - \tau) + D_S \Delta S - \delta RS, \\ \frac{dD}{dt} = 2(1 - p(D, a))S - (d + q(m))D + D_D \Delta D, \\ \frac{da}{dt} = a\left(\beta S \frac{a}{1+a} - \alpha\right) + D_a \Delta a, \\ \frac{dm}{dt} = \gamma e^{-S/S_0} - \alpha m + D_m \Delta m, \end{cases} \quad (12)$$

where δ is the cancer stem cells death rate by radiation therapy⁶⁶. In linear quadratic model, $R(t)$ can be defined as^{67,68}:

$$R(t) = \alpha_s d_t + 2\beta_s d_t \int_0^t d_t e^{-\mu(t-t')} dt', \quad (13)$$

where α_s and β_s are the sensitivity parameters. α_s corresponds to the cell that can not repair themselves after one radiation hit (important for high LET radiation) and β_s corresponds to cell that stop dividing after more then one radiation hit, but can repair the damage caused by radiation (important for low LET radiation), d_t is the dose-rate at time t , μ is the repair rate constant defined as $\frac{\ln(2)}{t_{1/2}}$ and $t_{1/2}$ is half-time for the repair of radiation-induced DNA damage. In fractional radiotherapy, dose is applied as fractions d_t for intervals $t_{2n-1} < t < t_{2n}$ where n is the fractions per day. In practice, dose fractions should be separated by 6 hours or more to permit repair to approach completion in late-responding tissues⁶⁹. Now, based on the studies conducted by Nilsson et al.⁷⁰ and Powathil et al.⁷¹ on the low-dose fractionated, Eq. (13) can be written as $R(t) = R_{eff} k_R$ where R_{eff} indicates the effect of n fractions per day and k_R is a factor equal to one when the radiation is applied and is equal to zero when no radiation is applied. The effective radiation can be written as:

$$R(t) = R_{eff} = \alpha_s(nD) + \beta_s n(D)^2 \left[g(\mu\tau_r) + 2 \left(\frac{\cosh(\mu\tau_r) - 1}{(\mu\tau_r)^2} \right) h_n(\phi) \right], \quad (14)$$

where τ_r is the duration of irradiation, D is the accumulated dose at time τ_r per fraction such that $D = d_t \tau_r$ and function $\phi = e^{-\mu(\tau_r + \Delta\tau_r)}$, where $\Delta\tau_r$ is the time interval between fractions. The functions $g(\mu\tau_r)$ and $h_c(\phi)$ are defined as:

$$g(\mu\tau_r) = 2 \frac{(\mu\tau_r - 1 + e^{-\mu\tau_r})}{(\mu\tau_r)^2}, \quad (15)$$

$$h_n(\phi) = 2 \frac{n\phi - n\phi^2 - \phi + \phi^{n+1}}{n(1 - \phi)^2}. \quad (16)$$

The function $g(\mu\tau_r)$ takes into account repair during fractions, the $h_n(\phi)$ function takes into account incomplete repair between fractions and $\left[g(\mu\tau_r) + 2 \left(\frac{\cosh(\mu\tau_r) - 1}{(\mu\tau_r)^2} \right) h_n(\phi) \right]$ is a function that corrects for both repair during the irradiation and incomplete repair between fractions.

Biological effective dose (BED): determination of the optimum dose

BED is the theoretical dose, which, if delivered in infinitely small fractions, would produce the same biological endpoint as that under consideration⁷². It is also a measure of the biological dose delivered to a tumor or organ. Treatment with any cytotoxic agent, including radiation can trigger surviving cells in tumor to divide faster than before, this phenomenon is called repopulation. Considering the proliferation of cancer stem cells during radiotherapy treatment from the LQ model⁷³, \log_e tumor cell kill E is given by

$$E = \alpha_s n \mathcal{D} \left(1 + \frac{\mathcal{D}}{\alpha_s / \beta_s} \right) \left[g(\mu\tau_r) + 2 \left(\frac{\cosh(\mu\tau_r) - 1}{(\mu\tau_r)^2} \right) h_n(\phi) \right] - K(T - T_d), \quad (17)$$

where T is the treatment time under consideration and T_d is the time after the start of treatment at which proliferation begins. K (in units of Gy/day) is the biological dose per day required to compensate for ongoing cancer stem cells repopulation, once this has started. K is the daily BED that must be delivered simply to stop the cancer stem cells growing further during treatment. The BED for the calculation of relationships in normal tissues defined by Barendsen⁷⁴ is given by

$$BED_{late} = n \mathcal{D} \left(1 + \frac{\mathcal{D}}{\theta_{late}} \right) \mathcal{M}, \quad (18)$$

where $\mathcal{M} = \left[g(\mu\tau_r) + 2 \left(\frac{\cosh(\mu\tau_r) - 1}{(\mu\tau_r)^2} \right) h_n(\phi) \right]$, θ_{late} is the α_s / β_s ratio for the normal tissue late effects and \mathcal{D} is again the accumulated dose at time τ_r , assumed to be the same for the cancer as for the adjacent critical normal tissues which is true in many practical situations. The consideration of the repopulation cancer stem cells effect is achieved through the use of a subtractive repopulation factor which takes account of the treatment and repopulation rate, the expression of BED is

$$BED_{can} = n \mathcal{D} \left(1 + \frac{\mathcal{D}}{\theta_{can}} \right) \mathcal{M} - K(T - T_d), \quad (19)$$

where θ_{can} is the α_s / β_s ratio for the cancer stem cells effects.

The relationship between n and T can be approximated as

$$T = fn - 1, \quad (20)$$

where f approximates to 7/5 for 5 fractions per week, providing more than 5 fractions are given⁷⁵. This form of approximation becomes more accurate when T is relatively large (greater than 14 days). Eq. (19) can be rewritten as

$$BED_{can} = \left(\frac{BED_{late}}{1 + \mathcal{D}/\theta_{late}} \right) \left(1 + \frac{\mathcal{D}}{\theta_{can}} \right) - K \left(f \frac{BED_{late}}{\mathcal{D}(1 + \mathcal{D}/\theta_{late}) \mathcal{M}} - 1 - T_d \right). \quad (21)$$

When the terms are rearranged and BED_{can} is differentiated with respect to \mathcal{D} , a dose per fraction given by the solution of

$$\left(1 - \frac{\theta_{late}}{\theta_{can}} \right) \mathcal{M} \mathcal{D}^2 - 2Kf\mathcal{D} - Kf\theta_{late} = 0. \quad (22)$$

The positive root of this quadratic equation provides the value of the optimum dose per fraction:

$$\mathcal{D}_{opt} = \frac{Kf + \sqrt{K^2 f^2 + (1 - \theta_{late}/\theta_{can}) Kf \theta_{late}}}{(1 - \theta_{late}/\theta_{can}) \mathcal{M}}. \quad (23)$$

We calculate the BED using the values of parameters in Table 2 and the values of radiobiological parameters for prostate cancer: $\theta_{late} = 3$ Gy, $T_d = 40$ days, $K = 0.2$ Gy/day⁷⁶ and $f = 7/5$ ⁷⁵. For a treatment time $T = 45$ days with 2 dose fractions per day, we obtain the values of the optimal dose and the BED given by

$$\mathcal{D}_{opt} = 1.328 \text{ Gy and } BED_{can} = 4.097 \text{ Gy} \quad (24)$$

respectively.

The tumor control probability (TCP)

The TCP is a key indicator to assess the effectiveness of cancer treatment⁷⁷. A higher TCP is generally associated with better outcomes and longer survival for patients. However, there are several factors that can influence

the TCP. The stage of cancer is one of these important factors, as indicates the extent of the disease. Early-stage tumors typically have a higher TCP than advanced-stage tumors. The location of tumor is also a factor to consider, as some tumors may be more challenging to treat due to their location in sensitive or hard-to-reach areas. The type of treatment used also plays a key role. Different types of treatments, such as surgery, radiotherapy and chemotherapy may have different effects on the tumor control probability. The patient's response to treatment is also an important factor. Each patient responds differently to treatments and how the body reacts can influence the tumor control probability. The (TCP) is the probability of avoiding local recurrence at total dose nD ⁷⁸. The Poisson's statistics and the linear-quadratic model incorporating the Poisson's law⁷⁹ lead to

$$TCP = \exp(-N.S_v) = \exp(-N \exp(-\alpha_s BED_{can})), \quad (25)$$

where $N = \zeta.V$ (ζ is cell concentration or density and V is volume) represents the initial number of potential proliferating cells in tumor and S_v is the cell survival probability such that $S_v = \exp(-\alpha_s BED_{can})$. The closer TCP is to one, the greater the probability that all cancer stem cells die out and the tumor is controlled⁸⁰. Spoormans et al.⁸¹ discussed that TCP takes into account the total absorbed dose and the radiosensitivity of the tumour tissue, while distinguishing between repairable and sublethal single-strand DNA breaks and irreparable and lethal double-strand DNA breaks. The parameters related to radiotherapeutic values are given in the Table 3.

Figure 6 shows the TCP as a function of fractionated dose D when the concentration S of cancer stem cells is equal to $0.000805 \text{ cell.mm}^{-3}$ at the starting time of the radiotherapy and for a prostate tumor that measures 8mm visible on magnetic resonance imaging⁸⁴. The volume of the tumor in the area ($100 \text{ mm} \times 100 \text{ mm}$) is 80000 mm^3 and when the prostate tumor measures 25 mm. The values of the parameters in the Table 3.

Figure 6 shows that the 2 dose fractions per day option requires 0.5273 Gy to avoid possible local resurgence of cancer after radiotherapy when tumor measures 8 mm. This requires 0.5697 Gy to avoid local resurgence after radiotherapy when tumor measures 25 mm.

Radiotherapy effects on the time series

Radiotherapy is one of the treatment modalities being substantially benefited in cancer research. Figures 7, 8 and 9 show the time series of S , D and m under the radiotherapy effects. The radiotherapy is applied at the time $t = 6.8964$ before the critical time delay $\tau_c = 11.8964$. The figures illustrate the changes in the concentration of prostate CSCs, DCs and microRNAs under the radiotherapy effects. We observe that the concentrations of CSCs and DCs decrease progressively with an increasing of the fractional dose. In contrast, the concentration

Parameter	Value/unit	References
α_s	0.302 Gy^{-1}	82
β_s	0.0417 Gy^{-2}	82
δ	$25 \text{ year}^{-1} \text{ Gy}^{-1}$	66
μ	$3195.77 \text{ year}^{-1}$	83

Table 3. Values of the radiobiological parameters.

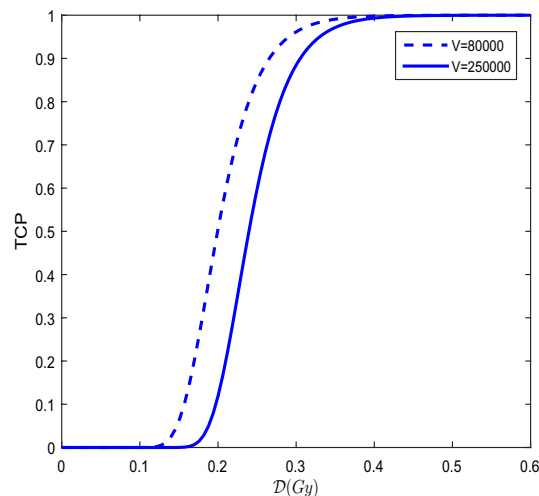


Figure 6. Evolution of TCP as a function of fractionated dose D for a treatment time $T= 45$ days, with 2 dose fractions per day when the prostate tumor volume is 80000 mm^3 (dashed line) and when the prostate tumor volume is 250000 mm^3 (solid line). That means the radiotherapy is applied on five successive days per week.

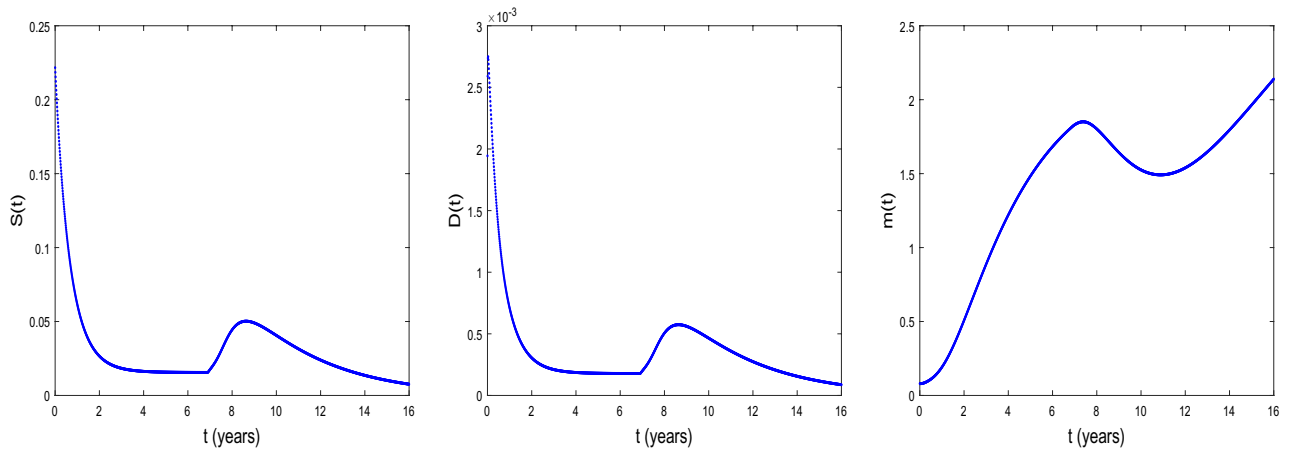


Figure 7. Time series of S, D and m under radiotherapy at $\tau = 6.8964 < \tau_c = 11.8964, t = 16$. $D_S = D_D = 0.0031536$ and $D_a = D_m = 0.036500$. $D = 0.02$ Gy, $n = 2$, $\tau_r = 0.000009$ year ~ 5 min and $\Delta\tau_r = 0.00069$ year ~ 6.04 h. The values of the other parameters are given in the Table 3.

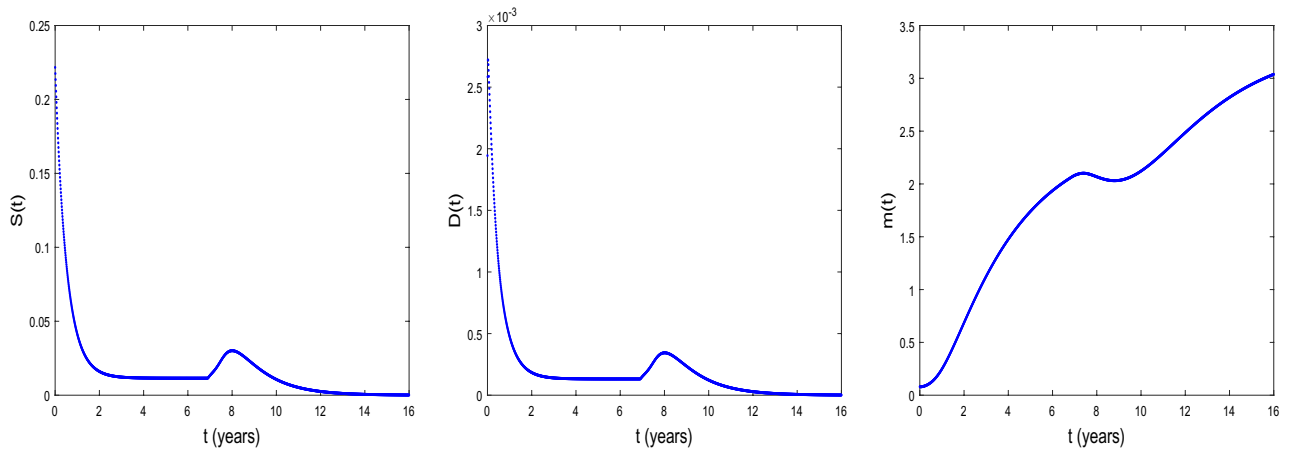


Figure 8. Time series of S, D and m under radiotherapy at $\tau = 6.8964 < \tau_c = 11.8964, t = 16$. $D_S = D_D = 0.0031536$ and $D_a = D_m = 0.036500$. $D = 0.05$ Gy, $n = 2$, $\tau_r = 0.000009$ year ~ 5 min and $\Delta\tau_r = 0.00069$ year ~ 6.04 h. The values of the other parameters are given in the Table 3.

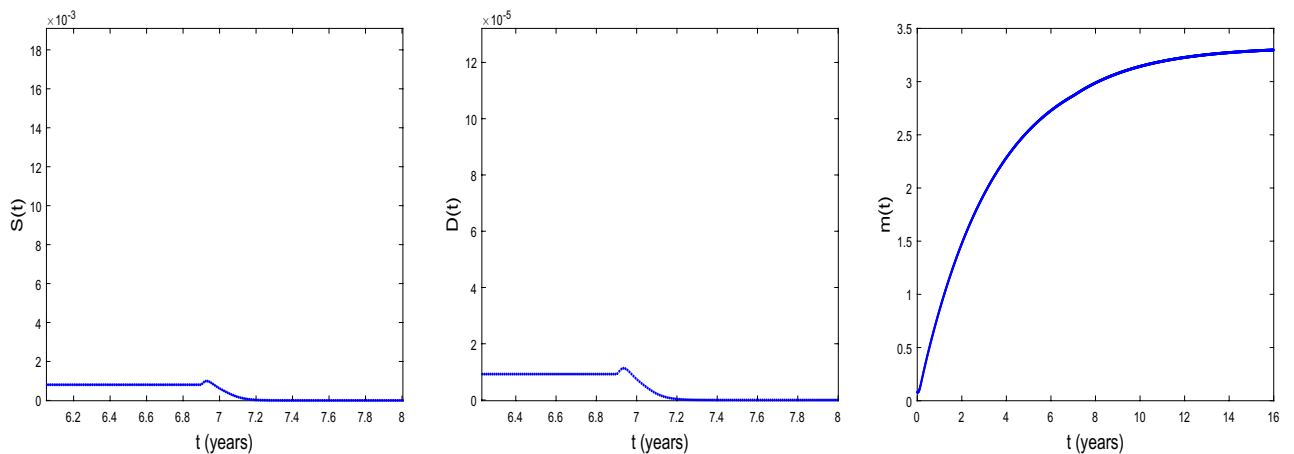


Figure 9. Time series of S, D and m under radiotherapy at $\tau = 6.8964 < \tau_c = 11.8964, t = 16$. $D_S = D_D = 0.0031536$ and $D_a = D_m = 0.036500$. $D = 1.323$ Gy, $n = 2$, $\tau_r = 0.000009$ year ~ 5 min and $\Delta\tau_r = 0.00069$ year ~ 6.04 h. The values of the other parameters are given in the Table 3.

of microRNAs increases when the fractional dose increases. This reflects the over-expression of microRNA under the radiotherapy effects as also found in⁸⁵. Along the same line, it has been shown that in prostate cancer patients, two microRNAs hsa-let-7a-5p and hsa-miR-21a-5p, were regulated by irradiation⁸⁶. Similarly, Halimi et al.⁸⁷ showed that irradiation during radiotherapy increases the serum miR-34a levels in 44 women with breast cancer. The obtained figures show that radiotherapy effects modify the expression of microRNAs and lead the CSCs to be radiosensitive to radiation. We also observe in these figures a tumor repopulation during radiotherapy. This confirms the results obtained in⁸⁸, where the investigators revealed that rapid tumor regrowth occurs during radiotherapy treatment extensions of around 5 to 8 weeks in almost 500 patients with oropharyngeal cancer⁸⁸. It is therefore necessary to administer a higher dose to regions of tumor repopulation for complete eradication of CSCs. In the present work, the CSCs are completely eradicated when the treatment lasts 0.3 year (~ 3.7) months for a dose of 1.323 Gy.

Radiotherapy effects on the pattern formation

This section is devoted to the radiotherapy effects on the patterns of cancer cell colony. To this end, we perform extensive numerical simulations of the mathematical model Eq. (12). The radiotherapy is applied at the time $t = 6.8964 > \tau_c = 11.8964$ before the critical time delay that is in the non-proliferation state of CSCs. Figures 10 and 11 illustrate the radiotherapy effects on the spatiotemporal dynamics of patterns. These figures show the changes in the prostate CSCs, DCs and microRNAs patterns when the dose of fractionated radiotherapy varies. In Fig. 10, we use the radiobiological values $\mathcal{D} = 0.02$ Gy, $n = 2$, $\tau_r = 0.000009$ year ~ 5 min and $\Delta\tau_r = 0.00069$ year ~ 6.04 h. We observe a partial eradication of patterns of CSCs and DCs and a decrease in the concentration level of cells as compared with Figs. 3 and 4. However, we observe an increase of the concentration level on the patterns of microRNAs leading to the fact that they can act as suppressor in certain tumors. In Fig. 11, we take $\mathcal{D} = 0.05$ Gy, that is, we increase the fractionated dose. In this case, the panels show a complete eradication of

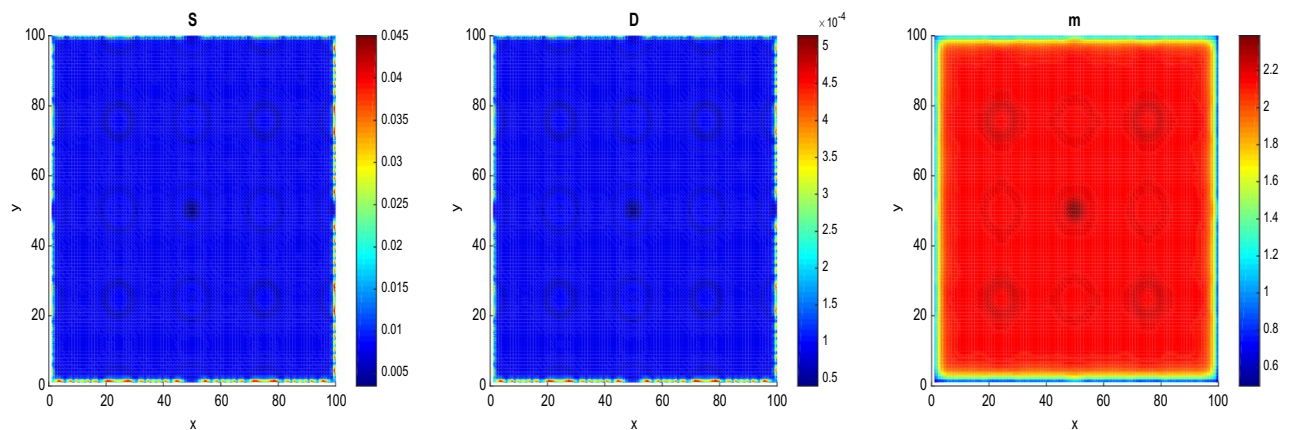


Figure 10. Behavior of S , D and m patterns under the radiotherapy at $\tau = 6.8964 < \tau_c = 11.8964$, $t = 16$. $D_S = D_D = 0.0031536$ and $D_a = D_m = 0.036500$. $\mathcal{D} = 0.02$ Gy, $n = 2$, $\tau_r = 0.000009$ year ~ 5 min and $\Delta\tau_r = 0.00069$ year ~ 6.04 h. The values of the other parameters are given in the Tables 1 and 3.

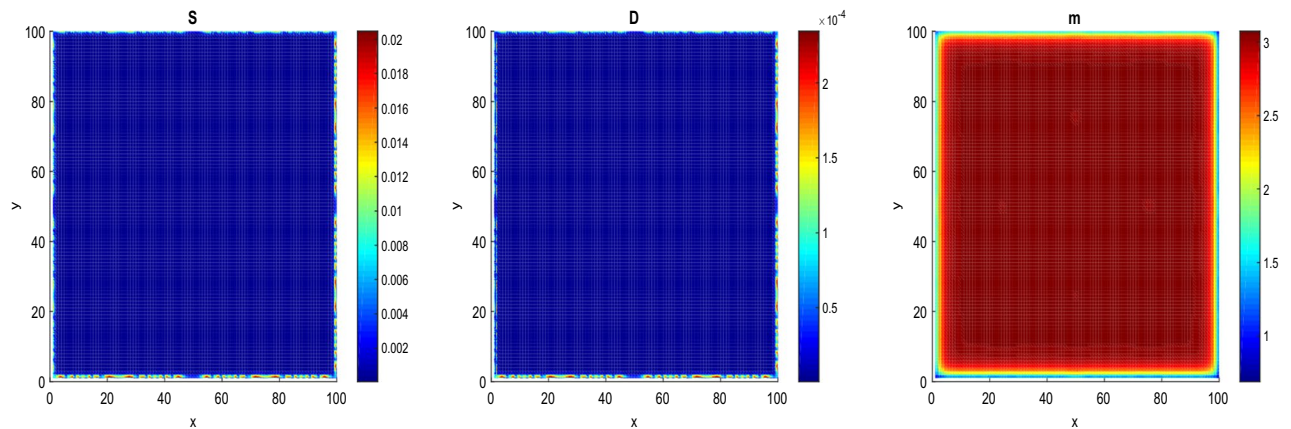


Figure 11. Behavior of S , D and m patterns under the radiotherapy at $\tau = 6.8964 < \tau_c = 11.8964$, $t = 16$. $D_S = D_D = 0.0031536$ and $D_a = D_m = 0.036500$. $\mathcal{D} = 0.05$ Gy, $n = 2$, $\tau_r = 0.000009$ year ~ 5 min and $\Delta\tau_r = 0.00069$ year ~ 6.04 h. The values of the other parameters are given in the Tables 1 and 3.

patterns of CSCs and DCs. The result obtained in this section clearly demonstrates that the administering of a therapeutic treatment, such as the radiotherapy, before the critical time delay τ_c , can lead to a complete eradication of the tumor.

Discussion and conclusion

In this paper, we studied a spatiotemporal dynamics of a diffusive model for CSCs. The model included the diffusion of CSCs, DCs, Wnt- β and microRNA molecules. The work focused on the critical time delay τ_c , since it represents the time from which some DCs transform into CSCs due to their interaction with microRNAs. We showed that the delayed model can induce a Hopf bifurcation and circular pattern formation. We have found that $\tau_c = 11.8964$ years for prostate cancer, $\tau_c = 0.6884$ year for lung cancer and $\tau_c = 0.5763$ year for breast cancer. As therapeutic strategy, radiotherapy effects have been included in the model and applied before τ_c . The results revealed that radiotherapy effects can completely eradicate cancer patterns and boost the suppressive effect of microRNAs on CSCs. The TCP curve showed that for the prostate tumor volumes equal to 80000 mm³ and 250000 mm³, for example, the respective maximum doses of 0.5354 Gy and 0.5758 Gy per dose fraction should be administered for a fractionation of 2 fractions per day. The results clearly illustrated that any resurgence of cancer at the same site after radiotherapy is not possible for a fraction of the dose required.

Before closing this work, it is important to point out the essential new features of this study with respect to some recent works for CSCs available in the literature^{18–20}. To start with, in¹⁸, the authors used a concept from ecology, the Allee effect, to demonstrate the effectiveness of combination therapies in cancer treatment compared to mono-therapy. In¹⁹, the authors studied clonal pattern dynamics in tumor in the concept of CSCs and showed that the most effective therapeutic strategies for tumor extinction are those that target chemical activators rather than cells themselves, due to a vicious feedback loop between CSCs and DCs. In²⁰, the authors investigated the dynamical model for CSCs taking into account the drug effects and showed some interesting mechanism, such as the tumor growth paradox, as possible outcome of therapy significantly. However, the works cited above and some other implicitly assume that biological transitions such as interactions between cancer cells with signaling molecules and proteins are instantaneous. In reality, the time delay exists between such interactions. This is important because DCs interact with microRNAs to transform into CSCs. In the present work, the proposed basic model illustrated this type of scenario. We showed that a diffusive model of CSCs with a time delay can be an effective modeling approach for therapeutic strategies. With the advancement of novel technology and methods, the circular patterns obtained numerically in this work have been found to give relevance biological significance. Just to cite a few, circular patterns have been identified to be extremely abundant, relatively stable, diverse, prevalent, and conserved in different diseases⁸⁹. Circular RNAs may aggregate in cells to induce pathologies, such as developmental and degenerative disorders⁹⁰. In addition, circular RNAs are expressed in a tissue-specific pattern, suggesting that they act as promising diagnostic and therapeutic value in management of cancer and various diseases^{76,91,92}. We clearly showed that the administering of a therapeutic treatment, such as the radiotherapy, before the critical time delay τ_c (that is during the non-proliferation phase of CSCs), can lead to a complete eradication of the tumor. This approach has the virtue of describing therapeutic strategies of the dynamics of CSCs with time delay. From that perspective, a wide range of phenomena in biology, physics and chemistry can be modeled by the present diffusive delayed system, and relevant applications to these areas may be proposed.

We hope that the results obtained in this work can provide a better understanding of the dynamics of CSCs and to predict more efficacy therapeutic strategies to prevent cancer recurrence.

Data availability

All data generated or analyzed during this study are included in this paper.

Received: 14 November 2023; Accepted: 21 February 2024

Published online: 04 March 2024

References

- Pranav, U. & Seshaiyer, P. Mathematical modeling, analysis, and simulation of tumor dynamics with drug interventions. *Bull. World Health Organ.* **81**(12), 917 (2003).
- Wang, Z. *et al.* Dynamic modeling of genes controlling cancer stem cell proliferation. *Front. In Genetics* **3**, 84 (2012).
- Visvader, J. E. & Lindeman, G. J. Cancer stem cells in solid tumours: Accumulating evidence and unresolved questions. *Nat. Rev. Cancer* **8**(10), 755–768 (2008).
- Driessens, G. *et al.* Defining the mode of tumour growth by clonal analysis. *Nature* **488**(7412), 527–530 (2012).
- Friedmann-Morvinski, D. & Verma, I. M. Dedifferentiation and reprogramming: Origins of cancer stem cells. *EMBO Rep.* **15**(3), 244–253 (2014).
- Lopez-Bertoni, H. *et al.* Bioreducible polymeric nanoparticles containing multiplexed cancer stem cell regulating mirnas inhibit glioblastoma growth and prolong survival. *Nano Lett.* **18**(7), 4086–4094 (2018).
- El Helou, R. *et al.* Mir-600 acts as a bimodal switch that regulates breast cancer stem cell fate through wnt signaling. *Cell Rep.* **18**(9), 2256–2268 (2017).
- Visvader, J. E. & Lindeman, G. J. Cancer stem cells in solid tumors: accumulating evidence and unresolved questions. *Nat. Rev. Cancer* **16**(3), 225–238 (2015).
- Sellerio, A. L. *et al.* Overshoot during phenotypic switching of cancer cell populations. *Sci. Rep.* **5**(1), 15464 (2015).
- Miyamae, M. *et al.* Plasma microRNA profiles: Identification of mir-744as a novel diagnostic and prognostic biomarker in pancreatic cancer. *Br. J. Cancer* **133**, 1467–1476 (2015).
- Liu, R. *et al.* Serum microRNA expression profile as a biomarker in diagnosis and prognosis of pancreatic cancer. *Clin. Chem.* **58**(3), 610–618 (2012).
- Shimomura, A. *et al.* Novel combination of serum microRNAs for detecting breast cancer in the early stage. *Cancer Sci.* **107**(3), 326–334 (2016).

13. Oreglia, M. *et al.* Early postoperative circulating mir-483-5p is a prognosis marker for adrenocortical cancer. *Cancers* **12**(3), 724 (2020).
14. Gebeshuber, C. A. *et al.* Mir-29a suppresses tritetrarprolin, which is a regulator of epithelial polarity and metastasis. *EMBO Rep.* **10**(4), 400–405 (2009).
15. Fabri, M. *et al.* MicroRNA-29 family reverts aberrant methylation in lung cancer by targeting DNA methyltransferases 3a and 3b. *Proc. Natl. Acad. Sci.* **104**(40), 15805–15810 (2007).
16. Bonnet, D. & Dick, J. E. Human acute myeloid leukemia is organized as hierarchy that originates from a primitive hematopoietic cell. *Nat. Med.* **3**(7), 730–737 (1997).
17. Wang, Z. *et al.* Network-based methods for the identification of microRNA-target pairs in cancer. *Brief. Bioinform.* **15**(6), 850–859 (2013).
18. Konstorum, A. *et al.* Feedback regulation in a cancer stem cell model can cause allee effect. *Bull. Math. Biol.* **78**(4), 754–785 (2016).
19. Olmeda, F. & Amar, M. B. Clonal pattern dynamics in tumor: The concept of cancer stem cells. *Sci. Rep.* **9**(1), 15607 (2019).
20. Mori, L. & Amar, M. B. Stochasticity and drug effects in dynamical model for cancer stem cells. *Cancers* **15**(677), 15607 (2023).
21. Pikovsky, A. & Rosenblum, A. Time-delayed feedback control of chaos in a population of coupled oscillators. *Phys. Rev. Lett.* **76**(11), 1804–1807 (1996).
22. Mvogo, A., Tiomela, S. A., Macías-Díaz, J. E. & Bodo, B. Dynamics of a cross-superdiffusive sirs model with delay effects in transmission and treatment. *Nonlinear Dyn.* **111**, 13619–13639 (2023).
23. Tiomela, S. A., Macías-Díaz, J. E. & Mvogo, A. Computer simulation of the dynamics of a spatial susceptible-infected-recovered epidemic model with time delays in transmission and treatment. *Comput. Methods Programs Biomed.* **212**, 106469 (2021).
24. Khan, F. M., & Gibbons, J. P. Khan's the Physics of Radiation Therapy 624 (2014).
25. Reya, T. *et al.* Stem cells and cancer stem cells. *Nature* **414**(6859), 105–111 (2001).
26. Lortz, A. *et al.* Populational adaptive evolution, chemotherapeutic resistance and multiple anti-cancer therapies. *Math. Model. Nat. Phenom.* **5**(3), 205–238 (2010).
27. Michor, P. *et al.* Dynamics of chronic myeloid leukaemia. *Nature* **435**(7046), 1267–1270 (2005).
28. Michor, F. Mathematical models of cancer stem cells. *J. Clin. Oncol.* **23**(31), 7930–7934 (2005).
29. Zhang, T. & Zang, H. Delay-induced Turing instability in reaction-diffusion equations. *Phys. Rev. E* **90**, 05208 (2014).
30. Shrabani, S. *et al.* Time-delay-induced instabilities in reaction-diffusion systems. *Phys. Rev. E* **80**, 046212 (2009).
31. Wang, X. *et al.* Delay-induced patterns in a reaction-diffusion system on complex networks. *New J. Phys.* **23**(7), 12 (2021).
32. Singh, S. K. *et al.* Identification of human brain tumour initiating cells. *Nature* **432**, 396–401 (2004).
33. Stephan, G. Delay effects in the human sensory system during balancing. *Philos. Trans. R. Soc. A Math. Phys. Eng. Sci.* **367**(1891), 1195–1212 (2009).
34. Weiss, L. D. *et al.* Determinants of stem cell enrichment in healthy tissues and tumors: Implications for non-genetic drug resistance. *bioRxiv*, 663146. <https://doi.org/10.1101/663146> (2019).
35. Li, C. *et al.* Identification of pancreatic cancer stem cells. *Cancer Res.* **7**(3), 1030–1037 (2007).
36. Lai, X. & Friedman, A. Exosomal mirs in lung cancer: A mathematical model. *Plos One* **11**(12), 0167706 (2016).
37. Cross, M. & Hohenberg, P. C. Pattern formation outside of equilibrium. *Math. Med. Biol.* **65**(3), 851 (1993).
38. Kaved, K., Kohandel, M. & Sivaloganathan, S. Replicator dynamics of cancer stem cells; Selection in the presence of differentiation and plasticity. *Math. Biosci.* **272**, 64–75 (2016).
39. Hillen, T., & Shintar, A. Modelling of cancer stem cell driven solid tumors, Education and Research Archive.
40. Watanabe, Y. *et al.* A mathematical model of tumor growth and its response to single irradiation. *Theor. Biol. Med. Modell.* **13**(6), 1–20 (2016).
41. Saijo, H. *et al.* plasticity of lung cancer -like cells is regulated by the transcription factor *hoxa5* that is induced by oxidative stress. *Oncotarget* **7**, 50043–50056 (2016).
42. Prayogo, A. A. *et al.* Dedifferentiation of mcf-7 breast cancer continuous cell line development of breast cancer stem cells (bcscs) enriched culture and biomarker analysis. *Indones. Biomed. J.* **12**(2), 185–188 (2020).
43. Enderling, H. *et al.* A mathematical model of breast cancer development, local treatment and recurrence. *J. Theor. Biol.* **246**(2), 245–256 (2007).
44. Hanahan, D. & Weinberg, R. A. The hallmarks of cancer. *Cell* **100**(1), 57–70 (2000).
45. Lamballe, F. *et al.* Modeling heterogeneity of triple-negative breast cancer uncovers a novel combinatorial treatment overcoming primary drug resistance. *Adv. Sci.* **8**(3), 2003049 (2020).
46. Deluche, E. *et al.* Contemporary outcomes of metastatic breast cancer among 22000 women from the multicentre esme cohort 2008–2016. *Eur. J. Cancer* **129**, 60–70 (2020).
47. Cao, W. *et al.* A review of biomarkers and their clinical impact in resected early-stage non-small-cell lung cancer. *Cancers* **15**(18), 4561 (2023).
48. Zeng, C. *et al.* Prognostic factors of patients with small cell lung cancer after surgical treatment. *Ann. Transl. Med.* **9**(14), 1146 (2021).
49. Pound, C. R. *et al.* Natural history of progression after PSA elevation following radical prostatectomy. *J. Am. Med. Assoc.* **281**(17), 1591–7 (1999).
50. Oberle, H. J. & Pesch, H. J. Numerical treatment of delay differential equations by hermite interpolation. *Numerische Mathematik* **37**, 235–255 (1981).
51. Ismail, F. *et al.* Numerical treatment of delay differential equations by Runge–Kutta method using hermite interpolation. *Matematika* **18**(2), 79–90 (2002).
52. Barbier, J. *et al.* An nf90/nf110-mediated feedback amplification loop regulates *dicer* expression and controls ovarian carcinoma progression. *Cell Res.* **47**, 201877 (2017).
53. Manit, S. R. *et al.* The metastatic cascade in prostate cancer. *Surg. Oncol.* **15**(13), 117–128 (2006).
54. Yan-Jing, Z. *et al.* Circular rnas negatively regulate cancer stem cells by physically binding *fmrp* against *ccar1* complex in hepatocellular carcinoma. *Theranostics* **9**(12), 3526–3540 (2019).
55. Mvogo, A., Ben-Bolie, G. H. & Kofané, T. C. Energy transport in the three coupled α -polypeptide chains of collagen molecule with long-range interactions effect. *Chaos* **25**(6), 063115 (2015).
56. Mvogo, A., Tambue, A., Ben-Bolie, G. H. & Kofané, T. C. Localized numerical impulse solutions in diffuse neural networks modeled by the complex fractional Ginzburg–Landau equation. *Commun. Nonlinear Sci. Numer. Simul.* **3**(8), 396–410 (2016).
57. Mvogo, A., Takembo, N. C., Ekobena, F. H. P. & Kofané, T. C. Pattern formation in diffusive excitable systems under magnetic flow effects. *Phys. Lett. A* **381**, 28 (2017).
58. Ritchie, J. Turing instability and pattern formation on directed networks. *Commun. Nonlinear Sci. Numer. Simul.* **116**, 106892 (2023).
59. Vo, J. N. *et al.* The landscape of circular RNA in cancer. *Cell* **176**(4), 869–881 (2019).
60. Kristensen, L. S. *et al.* The biogenesis, biology and characterization of circular RNAs. *Nat. Rev. Genet.* **20**, 675–691 (2019).
61. Henninger, J. *et al.* Clonal fate mapping quantifies the number of haematopoietic stem cells that arise during development. *Nat. Cell Biol.* **19**, 17–27 (2017).
62. Ginestier, C. H. K. *et al.* The cancer stem cell: The breast cancer driver. *Med. Sci.* **23**(12), 1133–1139 (2007).

63. Valbirk, K. C. *et al.* The role of cancer stem cells in tumor heterogeneity and resistance to therapy. *Can. J. Physiol. Pharmacol.* **95**(1), 1–15 (2017).
64. Bailleul-Dubois, J. & Bidan, N. The effect of radiotherapy on breast cancer stem cells: Resistance, reprogramming and treatments. *Oncology* **19**, 77–84 (2017).
65. Lan, T. *et al.* Cancer stem cells(cscs) in drug resistance and their therapeutic implications in cancer treatment. *Stem Cells Int.* 2018 (2018).
66. Chappell, M. *et al.* *Mathematical Modeling for Combinations of Immuno-Oncology and Anti-Cancer Therapies 14–17* (UK, Proceeding of the Report of the QSP UK meeting Macclesfield, 2015).
67. Sachs, R. *et al.* Simple ode models of tumor growth and anti-angiogenic or radiation treatment. *Math. Comput. Modell.* **33**, 1297–1305 (2001).
68. Tuzer, M., Yilmaz, D. & Unlu, M. B. Simulations on the efficacy of radiotherapy with different time schemes of antiangiogenic therapy. *BioRxiv* **9**(6), 459137 (2021).
69. Thames, J. H. D. Effet-independent measures of tissue responses to fractionated irradiation. *Int. J. Radiat. Biol. Relat. Stud. Phys. Chem. Med.* **45**(1), 1–10 (1984).
70. Nilsson, P. *et al.* A generalized formulation of the 'incomplete-repair' model for cell survival and tissue response to fractionated low dose-rate irradiation. *Int. J. f Radiat. Biol.* **57**(1), 127–142 (1990).
71. Powathil, G. *et al.* Mathematical modeling of brain tumors: Effects of radiotherapy and chemotherapy. *Phys. Med. Biol.* **52**(11), 3291 (2007).
72. Fowler, J. F. 21 Years of biologically effective dose. *Br. J. Radiol.* **83**(991), 554–568 (2010).
73. Fowler, J. F. The linear quadratic formula and progress in fractionated radiotherapy. *Br. J. Radiol.* **62**, 679–694 (1989).
74. Barendsen, G. W. Dose fractionation, dose rate and isoeffect relationships for normal tissue responses. *Int. J. Radiat. Oncol. Biol. Phys.* **8**(11), 1981–1997 (1982).
75. Jones, B., Tan, L. T. & Dale, R. G. Derivation of the optimum dose per fraction from the linear quadratic model. *Br. J. Radiol.* **68**(812), 894–902 (1995).
76. Zhuang, Q.-Y. *et al.* High biologically effective dose radiotherapy for brain metastases may improve survival and decrease risk for local relapse among patients with small-cell lung cancer: a propensity-matching analysis. *Cancer Control* **27**, 2 (2020).
77. Royce, T. J. *et al.* Tumor control probability and systematic review of the literature of stereotactic body radiotherapy for prostate cancer, International Journal of Radiation Oncology. *Biol. Phys.* **110**(1), 227–236 (2021).
78. Tucker, S. L., Thames, H. D. & Taylor, J. M. G. How well is the probability of tumour cure after fractionated irradiation described by poisson statistics?. *Radiat. Res.* **124**(3), 273–282 (1990).
79. Tomé, W. A. & Fowler, J. F. Selective boosting of tumour subvolumes. *Int. J. Radiat. Oncol. Biol. Phys.* **48**(2), 593–599 (2000).
80. Bachman Jeff, W. N. & Hillen, T. Mathematical optimization of the combination of radiation and differentiation therapies for cancer. *Front. Oncol.* **3**, 42398 (2013).
81. Spoormans, K. *et al.* A review on tumor control probability (tcp) and preclinical dosimetry in targeted radionuclide therapy (trt). *Pharmaceutics* **14**(10), 2007 (2022).
82. Yushi, W. *et al.* Treatment planning of carbon ion radiotherapy for prostate cancer based on cellular experiments with pc3 human prostate cancer cells. *Physica Medica* **107**, 102537 (2023).
83. Dasu, A. Toma-Dasu, Will infraction repair have negative consequences on extreme hypofractionation in prostate radiation therapy?. *Br. J. Radiol.* **88**, 0588 (2015).
84. Jiang, J. *et al.* Factors influencing the degree of enhancement of prostate cancer on contrast-enhanced transrectal ultrasonography: Correlation with biopsy and radical prostatectomy specimens. *Br. J. Radiol.* **85**(1019), 979–986 (2012).
85. Lin, J. *et al.* Mir-200c enhances radiosensitivity of human breast cancer cells. *Cell. Biochem.* **114**, 606–615 (2013).
86. Malla, B. *et al.* Protocol for serum mirnas analysis in prostate cancer patients treated with radiotherapy. *J. Transl. Med.* **16**, 223 (2018).
87. Halimi, M. *et al.* Human serum mir-34a as an indicator of exposure to ionizing radiation. *Radiat. Environ. Biophys.* **55**(5), 423–429 (2016).
88. Withers, H. R., Taylor, J. M. & Maciejewski, B. The hazard of accelerated tumor clonogen repopulation during radiotherapy. *Acta Oncologica* **27**, 131–146 (1988).
89. Sanger, H. *et al.* Viroids are single-stranded covalently closed circular RNA molecules existing as highly base-paired rod-like structures. *Proc. Natl. Acad. Sci.* **73**, 3852–6 (1976).
90. Yang, X. *et al.* Identification of circular RNA signature in bladder cancer. *J. Cancer* **8**, 3456–63 (2017).
91. Gao, D. *et al.* Screening circular RNA related to chemotherapeutic resistance in breast cancer. *Epigenomics* **9**, 1175–88 (2017).
92. Kreso, A. & Dick, J. Evolution of the cancer stem cell model. *Cell Stem Cell.* **14**, 275–91 (2014).

Author contributions

A.M. initiated the Project. F.E.E. performed the analytical results. F.E.E. and A.M. wrote the main manuscript text and prepared figures. A.M. and G.H.B.-B. performed numerical analysis. G.H.B.-B. supervised the manuscript. All authors reviewed the manuscript.

Competing interests

The authors declare no competing interests.

Additional information

Supplementary Information The online version contains supplementary material available at <https://doi.org/10.1038/s41598-024-55212-4>.

Correspondence and requests for materials should be addressed to A.M.

Reprints and permissions information is available at www.nature.com/reprints.

Publisher's note Springer Nature remains neutral with regard to jurisdictional claims in published maps and institutional affiliations.



Open Access This article is licensed under a Creative Commons Attribution 4.0 International License, which permits use, sharing, adaptation, distribution and reproduction in any medium or format, as long as you give appropriate credit to the original author(s) and the source, provide a link to the Creative Commons licence, and indicate if changes were made. The images or other third party material in this article are included in the article's Creative Commons licence, unless indicated otherwise in a credit line to the material. If material is not included in the article's Creative Commons licence and your intended use is not permitted by statutory regulation or exceeds the permitted use, you will need to obtain permission directly from the copyright holder. To view a copy of this licence, visit <http://creativecommons.org/licenses/by/4.0/>.

© The Author(s) 2024